A Nuclear Magnetic Resonance Study of Secondary and Tertiary Structure in Yeast $tRNA^{Phe}$†

G. T. Robillard,* C. E. Tarr,‡ F. Vosman,‡ and B. R. Reid

ABSTRACT: We present experimental evidence which confirms recently proposed ring current prediction methods for assigning hydrogen-bond proton nuclear magnetic resonance (NMR) spectra from tRNA (Robillard, G. T., Tarr, C. E., Vosman, F., & Berendsen, H. J. C. (1976) *Nature (London) 262,* 363-369; Robillard, G. T., Tarr, C. E., Vosman, F., & Sussman, J. L. (1977) *Biophys. Chem. 6,* 291-298). The evidence is a series of temperature-dependent studies on yeast $tRNA^{Phe}$ monitoring both the high- and low-field NMR spectral regions, which are correlated with independent optical and temperature-jump (temp-jump) studies performed under identical ionic strength conditions. Using assignments derived from the new prediction methods, the melting patterns of the hydrogen-bonded resonances agree with those expected on the basis of optical, temp-jump, and NMR studies on the high-field spectral region. The implication of these results is that previous assignment procedures are at least partially incorrect and, therefore, studies based on those procedures must be reexamined.

The application of proton magnetic resonance to elucidate the solution structure of tRNA has been focused almost exclusively on one spectral region, the low-field region containing resonances from hydrogen-bonded protons. Resonances of covalently bound protons which do not exchange with solvent can be assigned from model compounds. In contrast, resonances from hydrogen-bonded protons can only be observed as long as the hydrogen bond remains intact. Since the stability of such bonds in H_2O is low the resonances are difficult to observe in model systems. When they can be observed their chemical-shift positions are a composite of several parameters whose individual contributions are difficult to assess.

From studies on yeast $tRNA^{Phe}$ and other tRNA species, Shulman et al. (1973) developed a semiempirical method for assigning hydrogen-bonded proton resonances in tRNA nuclear magnetic resonance (NMR) spectra. Using ring current values extrapolated from Giessner-Prettre and Pullman's isoshielding contours (1970) and Arnott's models of ideal stacking in ribonucleotide double helices (1971), tables were computed which listed the shift of the ring NH-ring N hydrogen-bonded proton as a function of the composition of the neighboring bases (Shulman et al., 1973). A fundamental assumption in generating these tables was that the observed resonances arose only from Watson-Crick type hydrogen-bonding arrangements. The result was that all resonances below −13.6 ppm were assigned to Watson-crick A·U interactions. Since resonances were originally found as low as −14.4 ppm, the unshifted position for an A·U hydrogen-bonded proton resonance was placed at −14.8 ppm. When checked against the fragment studies of Lightfoot et al. (1973) reasonable agreement was found between the observed and predicted spectral positions. These studies, however, were carried out prior to the solution of the x-ray crystal structure of yeast $tRNA^{Phe}$. Due to incorrect integration of the spectra only 19 proton resonances were found in the low-field regions, a number in good agreement with the 20 resonances expected from secondary structure interactions in the cloverleaf (Lightfoot et al., 1973; Kearns & Shulman, 1974).

In 1974 the x-ray crystallographic studies on yeast $tRNA^{Phe}$ demonstrated the presence of tertiary structure ring NH-ring N type hydrogen bonds (Kim et al., 1974; Robertus et al., 1974). Subsequent NMR studies at higher resolution have clearly shown that NMR spectra of virtually all class I tRNAs contain resonances from 5 to 7 of these tertiary structure interactions in the low-field spectral region (Reid et al., 1975, 1977; Reid & Robillard, 1975; Robillard et al., 1976b). One resonance in the very-low-field spectral region was experimentally assigned to the reversed Hoogstein s^4U-8-A-14 interaction (Wong et al., 1975a,b; Reid et al., 1975). In both studies, the removal of the sulfur from s^4U8 caused the loss of a resonance at −14.9 ppm and the appearance of a new one at −14.3 ppm belonging to a normal A·U reversed Hoogstein interaction.

Virtually all class I tRNA NMR spectra published to date contain only one or two resonances below −14 ppm. In light of the above chemical modification results and the fact that essentially all class I tRNAs have two reversed Hoogstein interactions, one must consider the possibility that the resonances in tRNA NMR spectra below −14 ppm arise from non-Watson-Crick type A·U interactions while resonances from Watson-Crick type A·U interactions usually appear above −14 ppm. If such a possibility were correct, it would imply that all previous interpretations of tRNA NMR spectra based on earlier prediction methods are at least partially incorrect and require reexamination.

In recent studies we have found that NMR spectra of yeast $tRNA^{Phe}$ and *Escherichia coli* $tRNA^{Val}_1$ can be computed from x-ray crystal-structure coordinates and show remarkable similarity to the observed spectra (Robillard et al., 1976b,

† From the Department of Physical Chemistry, University of Groningen, Groningen, The Netherlands (G.T.R., C.E.T., F.V.), and the Department of Biochemistry, University of California, Riverside, California 92502 (B.R.R.). *Received April 12, 1977.* We wish to acknowledge the ZWO (Netherlands Foundation for the Advancement of Pure Research) for their support of the high-resolution NMR facility at the University of Groningen. This work has been presented, in part, at the British Biophysical Society Meeting on NMR in Biology, March 1977, Oxford, England.

In a preliminary account of this work, [Dwek et al., Ed. (1977) *NMR in Biology,* Academic Press, New York, N.Y.] the chemical shifts of the methyl resonances are reported 0.2 ppm to higher field than they should be due to an incorrect determination of the deuterium lock frequency. In addition, the assignments listed in the 48 °C spectrum, Figure 7A of the same account, are incorrectly attributed to Kan et al. (1974) through an editorial error.

‡ Present address: Department of Physicis, University of Maine, Orono, Maine 04473.

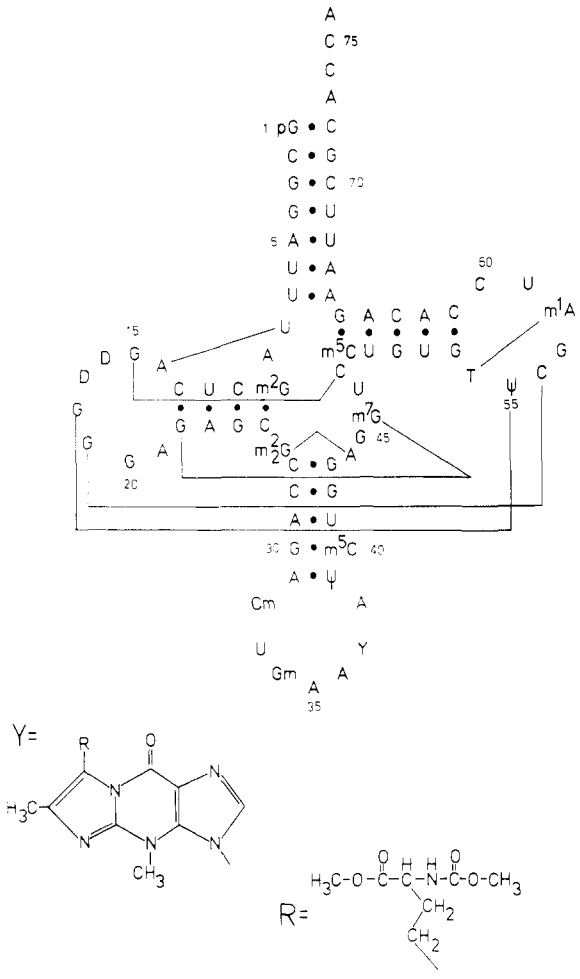

FIGURE 1: Cloverleaf sequence of yeast $tRNA^{Phe}$. The solid lines indicate the tertiary structure interactions determined crystallographically (Kim et al., 1974; Robertus et al., 1974) which, we suggest, give rise to hydrogen-bonded proton resonances below −11 ppm in the NMR spectrum of yeast $tRNA^{Phe}$.

1977). This agreement is obtained only if the above-mentioned change in the low-field starting position for the A·U resonances is made and ring current values quite similar to those published by Giessner-Prettre and Pullman (1965) are used. If, on the other hand, the original low-field starting positions and the increased ring current shift parameters (Shulman et al., 1973) are used, the same calculations do not give any noticeable agreement with the experimental spectra. While the results of these calculations support the new prediction procedures, they contain several assumptions and approximations. Therefore, experimental proof is also required.

In the present study we show how the assignments predicted by these calculations agree with the resonances lost during the melting transitions observed by temperature-dependent NMR studies on the high- and low-field spectral region, thereby providing the experimental support for these new prediction procedures.

Materials and Methods

Yeast $tRNA^{Phe}$. Two sources were used. High-field spectra were obtained using commercially available samples from Boehringer Mannheim. No difference was observed between these spectra and spectra taken with a highly purified sample supplied by Professor G. Dirheimer (Strasbourg). Low-field spectra were obtained using either commercial samples or samples purified by BD-cellulose chromatography (Gillam et

FIGURE 2: 360-MHz proton NMR spectra of 5×10^{-4} M yeast $tRNA^{Phe}$ taken at various temperatures. The sample was dialyzed against 15 mM $MgCl_2$-0.1 M NaCl in D_2O, pH 7 (meter reading), for 48 h. The spectra do not represent the same number of sweeps.

al., 1967) followed by DEAE-Sephadex[1] chromatography (Nishimura, 1971) followed by Sepharose chromatography (Holmes et al., 1975). The resulting material was homogeneous as judged by RNase fingerprinting and the stoichiometry of aminocylation using pure yeast $tRNA^{Phe}$ synthetase (Schmidt et al., 1971).

Preparation of NMR Samples. tRNA (5 mg) was dissolved in 1 mL of H_2O and dialyzed at 5 °C for 48 h against 4 volumes of the buffer specified in the figure legend. In the case of samples where Mg^{2+} was removed, the tRNA was first dialyzed for 48 h in the buffer specified which also contained 10 mM EDTA. This was followed by dialysis for 48 h in the absence of EDTA. The samples were then concentrated to NMR volumes by vacuum dialysis. Following this procedure reproducible NMR spectra could be obtained. This is an especially difficult problem when working in low salt in the absence of Mg^{2+}.

Samples used for measurements in the high-field spectral region were treated in the same manner as above; however, the buffers were prepared in D_2O. In these cases the stated pH refers to a pH meter reading.

Nuclease Digestion. A total of 40 units of Merck T_1 RNase and 40 μg of bovine pancreatic RNase (Miles) in a 20-μL volume of D_2O was added to the NMR sample. After heating the sample in a 50 °C water bath for 24 h, the NMR spectrum was measured.

NMR Spectra. NMR spectra were taken using either correlation spectroscopy (sweep rate = 1 kHz/s) or Fourier transform (60° pulse, 1.6-s acquisition time and 10-s pulse delay) procedures on a Bruker HX 360-MHz spectrometer. The field was locked to D_2O in the solvent. Samples in H_2O

[1] Abbreviations used are: DEAE, diethylaminoethyl; EDTA, ethylenediaminetetraacetic acid; DSS, sodium 4,4-dimethyl-4-silapentane-5-sulfonate; temp-jump, temperature jump.

TABLE I: Transitions Observed during the Thermal Denaturation of Yeast $tRNA^{Phe}$ in 30 mM Na^+, no Mg^{2+}, pH 6.8.

Transition	Structure involved	T_m, (°C)	Relaxation time	Reference
1	Tertiary structure	25	Slow: 10 ms	Romer et al., 1970
2 and 3	Residual tertiary structure Acceptor stem Anticodon helix	35-40	Slow: 2-23 ms & 17-475 ms	Coutts et al., 1975
4	TΨC helix	45-50	Fast: 20-100 μs	Romer et al., 1969
5	D helix	60-65	Fast: 20-100 μs	Romer et al., 1969

contained 2% D_2O for locking. Chemical-shift positions were determined for the high-field spectral region using duplicate samples containing sodium 4,4-dimethyl-4-silapentane-5-sulfonate (DSS). In the low-field spectral region the chemical shift was measured relative to H_2O and extrapolated to DSS using a plot of the chemical shift of water relative to DSS vs. temperature.

Spectral Integration. Two procedures have been employed: (i) measuring the area by counting cm^2 on the original spectrum; (ii) using a computer program which allows one to subtract a Lorentzian line of specified height and width from the stored spectrum while simultaneously providing a printout of the chemical shift and area of the subtracted peak.

Results and Interpretation

Experimental Approach. Resonances from methylated bases were first observed in the high-field region of the tRNA NMR spectrum by Smith et al. (1969). In the case of yeast $tRNA^{Phe}$ these resonances were assigned by Kan et al. (1974) via NMR studies on the component bases. Since there is very little ambiguity in these resonance assignments, the melting transitions of yeast $tRNA^{Phe}$ have been defined, in this study, by monitoring the temperature dependence of the high-field spectral region. These studies were performed at pH and ionic strengths identical with those used in an extensive series of temp-jump optical and fluorescence studies (Romer et al., 1969, 1970; Riesner et al., 1973; Urbanke et al., 1975; Coutts et al., 1975). Since the T_m values and assignments of transitions are identical for the two studies the data have been combined to define the sequence of melting which will be observed in the low-field spectral region under identical solvent conditions. Resonances lost from the low-field spectra during these transitions are then correlated with assignments made by the new prediction procedures. By this approach the circularity of defining melting transitions and determining the accuracy of the resonance assignments on the basis of these transitions is eliminated.

Information from Modified Bases. The high-field region of the proton NMR spectrum of yeast $tRNA^{Phe}$ contains only resonances arising from methyl and methylene groups of modified bases. Since there is an even distribution of these bases in the anticodon, TΨC, and D stem and loop regions, including places where a number of crystallographically determined tertiary interactions have been demonstrated (see Figure 1), the temperature dependence of these methyl resonances was monitored as a probe for secondary and tertiary structure transitions. Figure 2 presents 360-MHz NMR spectra in the high-field region for yeast $tRNA^{Phe}$ in 15 mM Mg^{2+}-0.1 M NaCl (pH 7) in D_2O. Each resonance between 0 and −3.5 ppm is well resolved. Other than the slight shifts observed near −3.6 ppm both the integrated intensity and the resonance positions of each resonance remain the same in the temperature range from 35 to 65 °C. Between 65 and 75 °C an abrupt and irreversible change occurs resulting in a largely different spectrum with essentially the same integrated intensity.

Romer et al. (1970) demonstrated that, in the presence of Mg^{2+}, yeast $tRNA^{Phe}$ melts in a single cooperative transition between 65 and 75 °C. This is identical with the transition observed by NMR in Figure 2. These investigators also reported that, in 30 mM Na^+, after removal of Mg^{2+}, the melting of yeast $tRNA^{Phe}$ could be resolved into five transitions (see Table I) occurring over a range between 20 and 70 °C. In order to observe the individual structural transitions by NMR, measurements under similar solvent conditions were performed.

The temperature dependences of the high-field NMR spectra of yeast $tRNA^{Phe}$ in 30 mM Na^+, no Mg^{2+}, pH 6.8, are presented in Figure 3. At the lowest temperature the spectrum is essentially identical with that observed in the presence of Mg^{2+} between 35 and 65 °C (see Figure 2). Nevertheless, the structure is less stable in the 30 mM Na^+-Mg^{2+} free buffer and, under these conditions, the tRNA undergoes three separate thermal transitions which we shall refer to as transitions I, II, and III. Transition I is a slow exchange transition occurring between 20 and 40 °C (Figure 3A) affecting a large proportion of the resonances between 0 and −3.7 ppm. The slow exchange between these two states is reflected in the disappearance of some resonances with the concomitant appearance of others. A detailed consideration of this transition will be presented shortly. Transition II is reported only by the T-54 methyl. It is a fast exchange transition with an apparent T_M of 40 to 50 °C (see Figure 4). Transition III occurs between 50 and 90 °C (Figure 3B). It is rapid on the NMR time scale as reflected in the smooth shifting of certain resonance positions as a function of temperature. After 80 °C there are no further spectral changes and the molecule appears to be in a completely random coil form. The assignments listed on the 80 °C spectrum are those presented by Kan et al. (1974). For the sake of clarity we will consider the transitions in the reverse order beginning with the high-temperature spectra where the resonance assignments are most certain.

Transition III, 50 to 80 °C. Figure 5 compares an 80 °C spectrum (C) of yeast $tRNA^{Phe}$ in 30 mM Na^+ with a 30 °C spectrum (B) of the same sample after it had been incubated at 50 °C for 24 h in the presence of a mixture of pancreatic and T_1 RNase (see Materials and Methods). With the exception of slight temperature-dependent shifts in resonance positions and the merging of the resonances of m^5C-40 and m^5C-49, the spectra are similar, showing that the 80 °C spectrum of intact yeast $tRNA^{Phe}$ portrays the random-coil form of the molecule where each base is effectively free in solution.

As the temperature is lowered we see in Figures 3B and 4 that structural reorganization is first reported by the upfield shifts of resonances from the two dihydrouridine bases and m_2^2G-26 with an apparent T_M of 60–65 °C. At 60 °C the resonances of the m_2^2G-26 and the dihydrouridines are superimposed. Therefore the assignments at lower temperature,

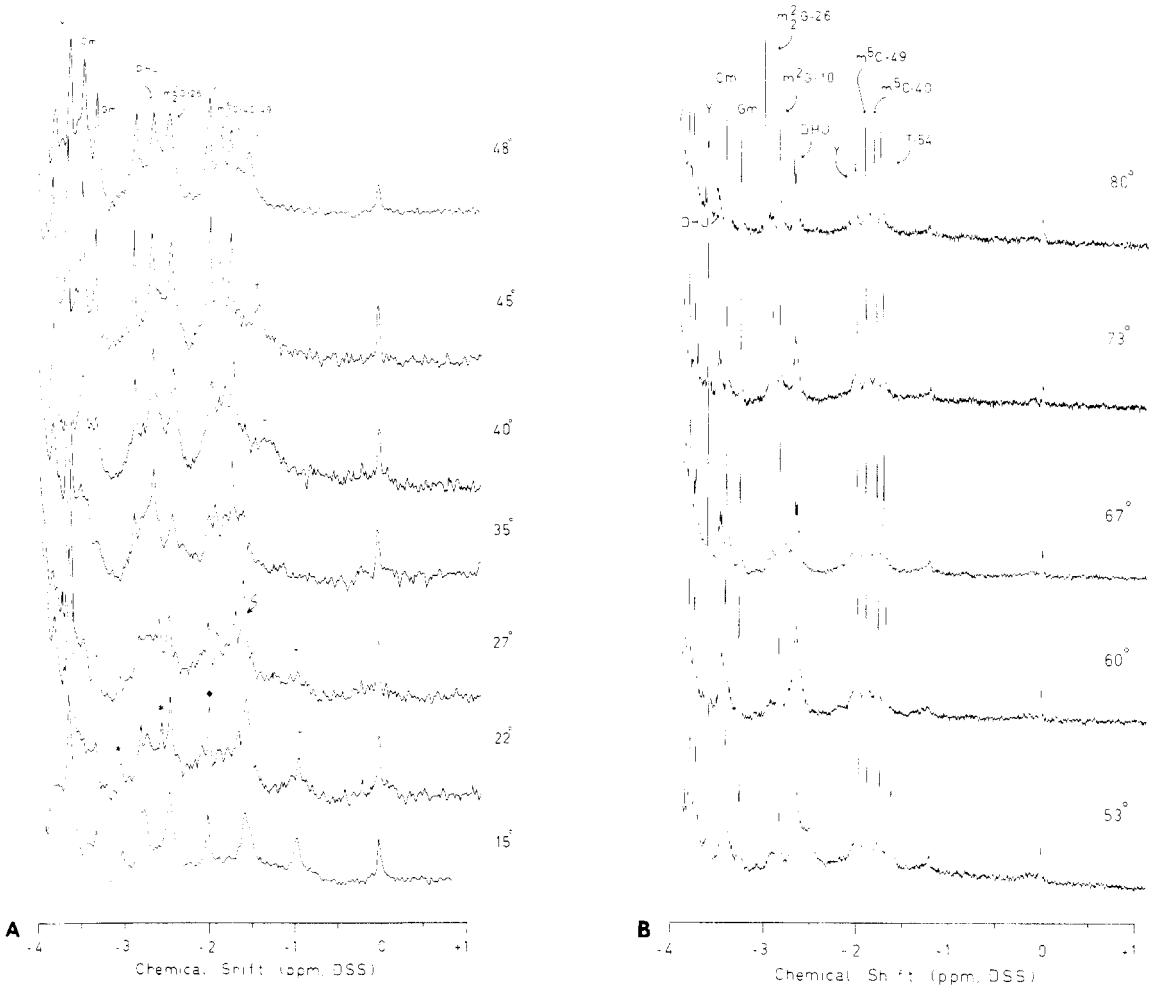

FIGURE 3: 360-MHz NMR spectra of Mg^{2+} free yeast $tRNA^{Phe}$ (2×10^{-4} M) in 10 mM NaD_2PO_4–20 mM NaCl (pH 6.8) as a function of temperature: (A) temperature 15–48 °C; the assignments in the 48 °C spectrum are taken from Kan et al. (1974) except for the DHU and m_2^2G-26 assignments which have been reversed as discussed in the text; (B) temperature, 51–80 °C; the assignments in the 80 °C spectrum are taken from Kan et al. (1974). In section A the 15 and 48 °C spectra have been signal averaged longer than the rest for an improved signal-to-noise ratio.

when the peaks separate, are ambiguous. The assignments we have made show that the DHU shifts only slightly while the m_2^2G-26 resonance shifts extensively beginning on the low-field side of the DHU resonance and moving to the high-field side as the temperature is lowered. These assignments are based on the following double irradiation experiments.

Spectrum A in Figure 5 shows that dihydrouridine has a complex spectrum in the high-field region resulting from the spin coupling of the C_5 and C_6 methylene protons. These multiplets are visible in the spectrum (B) of the ribonuclease treated sample as well as in the 80 °C spectrum of the intact tRNA (spectrum C). Irradiation of one of these DHU multiplets will cause a decoupling and concomitant sharpening of the other multiplet. The DHU resonance at −3.5 ppm in Figure 5C moves slightly upfield at lower temperatures and moves under the peak at −3.45 ppm (see Figure 3B). When this peak is irradiated (spectrum C, Figure 6) the resonance at −2.65 ppm, indicated by the arrow, nearly doubles in height relative to that same peak when there is no irradiation (spectrum A) or where the point of irradiation is 20 Hz off resonance (spectrum B). These results prove conclusively that the peak at −2.65 ppm in Figure 6 belongs to the DHU and the peak to the right of it can be assigned to the m_2^2G-26.

Therefore, in transition III the DHU resonances experience only very slight shifts while the methyl resonances of m_2^2G-26 are shifted extensively. It should be emphasized that these resonances of the DHU and m_2^2G-26 have the same T_m of 60 to 65 °C in transition III as can be seen from the plot in Figure 4 suggesting that they are reporting the same structural event. Romer et al. (1969, 1970) observe an optical transiton with a T_m of 60–65 °C (see Table I) in the isolated 5′ half-fragment and assigned the transition to the unwinding of the D helix in complete agreement with the shifts of the dihydrouridine methylenes and m_2^2G-26 methyl protons.

Transition II, 45–55 °C. The methyl group of T-54 senses at least two different environments while passing through the temperature range from 20 to 80 °C. In the range of transition III there is a very gradual shift 0.1 ppm upfield. Between 55 and 40 °C, however, there is a distinct transition with an apparent T_m of 45–50 °C resulting in a further upfield shift of 0.37 ppm. Since this transition is not reported by any other methyl resonances in these spectra it suggests that the events being sensed may be local changes in the TΨC loop and helix following the structural changes which occur in transition I discussed below. As seen in Table I the T_m of transition II correlates with the melting of the TΨC helix observed to occur at 45 to 50 °C by optical studies on the 3′ half-molecule fragment. The relaxation time of this transition also agrees with the smooth shifting of the thymine resonance observed in Figure 4. The thymine shifts approximately 0.4 ppm in transition II. With a chemical-shift difference between two states of 0.4 ppm the exchange time between the two states must be faster than ~500 μs for a resonance to be shifting in the fast exchange limit. The relaxation time of transition 4 in Table I

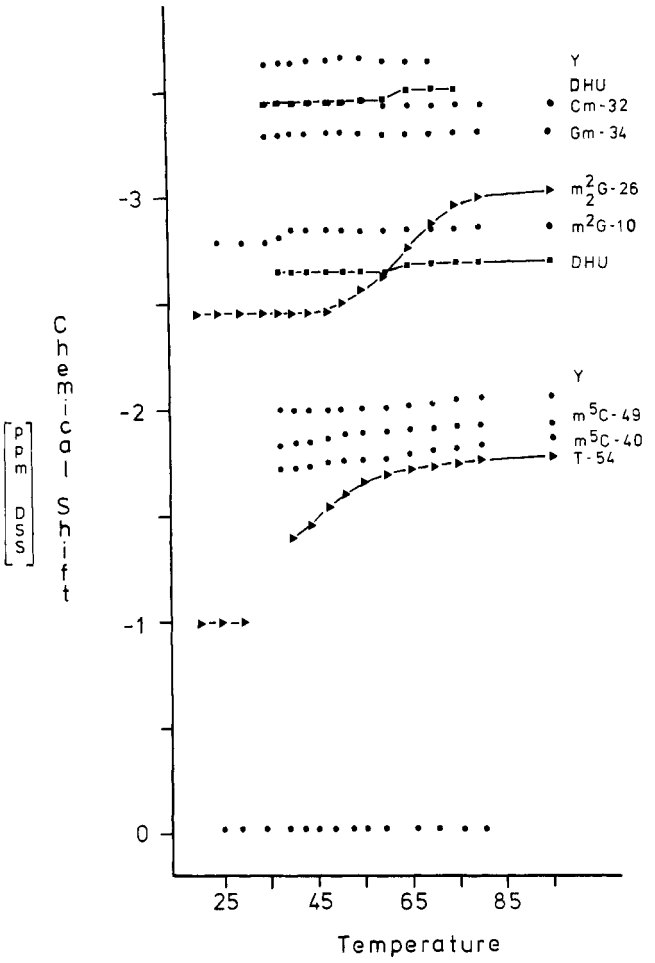

FIGURE 4: Plot of the chemical shift as a function of temperature for the resonances in Figures 3A and 3B.

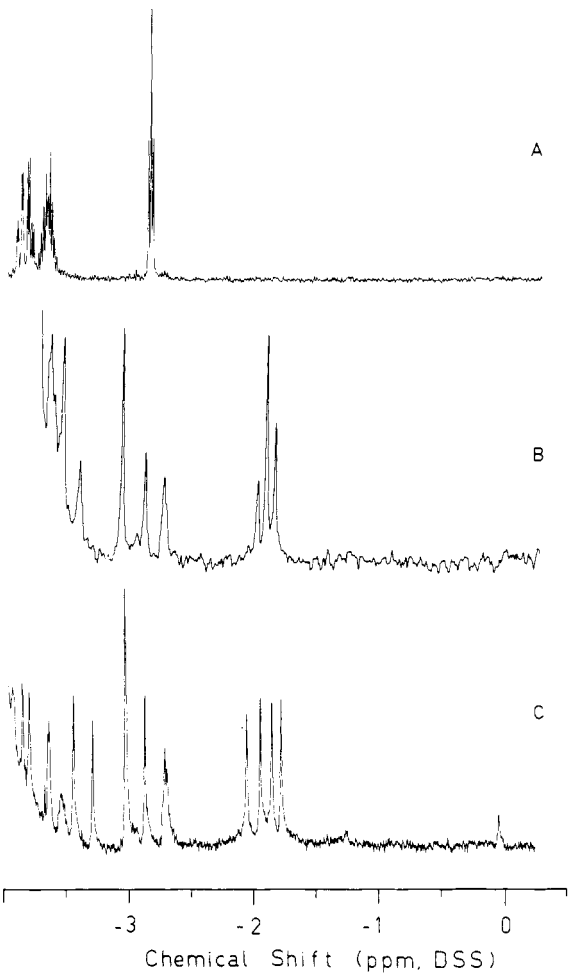

FIGURE 5: 360-MHz proton NMR spectra of: (A) dihydrouridine in 10 mM NaD_2PO_4–20 mM NaCl (pH 6.8); (B) yeast $tRNA^{Phe}$ after treatment with RNase; (C) yeast $tRNA^{Phe}$ in 10 mM NaD_2PO_4–20 mM NaCl (pH 6.8) at 80 °C.

is 20–100 μs, thus agreeing with the fast exchange type shifting observed for the thymine resonance.

Transition I, 20 to 40 °C. The 45 °C spectrum in Figure 3A shows the methyl resonance of T-54 beginning to decrease in intensity and broaden as the temperature is lowered. Its disappearance reflects the thymine methyl going from the fast exchange limit into intermediate exchange. The resonance finally reappears in the 27 °C spectrum shifted upfield to −1.0 ppm. The change in position is reporting an intermediate or slow exchange conversion between two structures in the 20 to 40 °C range. A similar decrease in intensity is observed for the resonances from m^5C-40 and m^5C-49 in the 45 °C spectra with a corresponding increase of the resonance just upfield marked by the arrow in the 27 °C spectrum. The Y base resonance at −2.06 ppm undergoes a similar change and, in this case, is shifted downfield to the position marked by the diamond in the 22 °C spectrum. The region between −2.4 and −3.1 ppm has essentially the same integrated intensity at 15 and 48 °C. Nevertheless, this region also shows changes between two states as seen by the disappearance of the DHU resonance at −2.65 ppm and the corresponding increase or shifts of the resonances marked by asterisks. The region below −3.1 ppm, where resonances of DHU, Cm-32, Gm-34, and the methyl esters of the Y base occur, also reflects a slow exchange between two states as seen by the decrease in the intensity of Cm-32 and Gm-34 and the increase in intensity of the peak at −3.65 ppm. The only case of a resonance shifting in the fast exchange limit during transition I is m^2G-10. Since it experiences a shift of approximately 0.1 ppm the exchange time between the two states would have to be 2 ms or faster. Table I shows that processes with these lifetimes are occurring in transitions 2 or 3.

In general the 20 to 40 °C temperature dependence of the methyl resonances in the high-field spectrum suggests that, in transition I, the molecule is undergoing quite widespread structural alterations involving the D, TΨC and anticodon helix and loop regions as well as the junction between these arms. Referring again to Table I we see that the three lowest temperature transitions observed optically occur with T_ms of 25 and 35 °C and involve the opening of tertiary structure and the anticodon and acceptor helices. Furthermore, the relaxation times of these transitions are slow. The methyl resonances reporting transition I arise from methylated bases participating either in tertiary structure interactions or in the secondary structure of the anticodon helix and loop. Because of the broad temperature range between the beginning and end of transition I, however, it is not possible to separately monitor the two T_ms observed optically. Nevertheless, it appears that the same events monitored by optical melting or temp-jump techniques are being reported by the methyl resonance spectra. In addition, the events occur in the same sequence for both sets of measurements.

Hydrogen-Bonded Proton Resonances. Spectral Integration. Figure 7 compares an NMR spectrum of yeast $tRNA^{Phe}$ dialyzed against 20 mM KH_2PO_4–5 × 10^{-4} M $MgCl_2$ (pH 7) (spectrum A) with the spectrum of the molecule after all

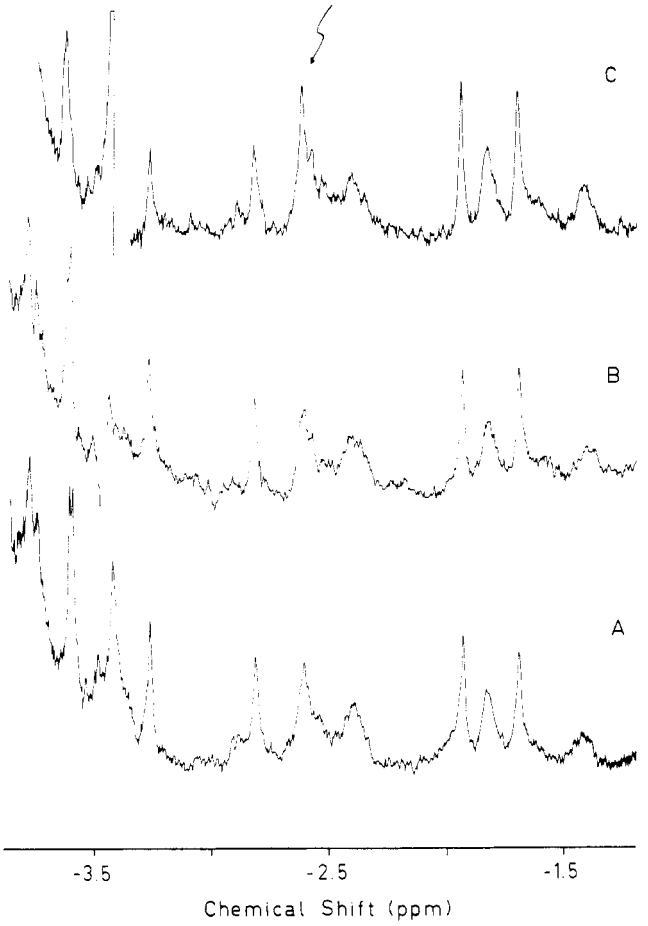

FIGURE 6: Effects of double irradiation on the high-field spectral region of yeast $tRNA^{Phe}$ in 30 mM Na, no Mg^{2+}, pH 6.8, 45 °C. Spectra were taken in the Fourier transform mode using a decoupling pulse width of 5 μs and 1-W decoupling power: (A) decoupler off; (B) decoupler on; decoupling frequency set 20 Hz below −3.45 ppm; (C) decoupler on; decoupling frequency set at −3.45 ppm. The arrow at −2.6 ppm indicates the decoupled DHU resonance.

Mg^{2+} has been removed by dialysis against EDTA (spectrum B). The intensity of spectrum A has been determined by a computer program as described under Materials and Methods. Choosing the height and width from any one of the smallest resolved resonances in spectrum A, the program found a total of 26 resonances in the region between −11 and −15 ppm. When Mg^{2+} is removed by dialysis vs. EDTA the spectrum (B) showed only one change of integrated intensity between −11 and −15 ppm. Peak C which contained five proton resonances in spectrum A contains only four proton resonances in this spectrum. In spite of slight shifts in resonance positions between the spectra, the integrated intensity of all other regions remains the same. The calculated resonance positions listed below spectrum A are based on atomic coordinates from the x-ray crystal-structure (Sussman & Kim, 1975) and ring current calculations using the new AU° positions (Robillard et al., 1976b). They are presented here since we will be referring to them in the following analysis.

Thermal Denaturation. Figure 8 presents the temperature dependence of yeast $tRNA^{Phe}$ in the absence of Mg^{2+} as seen in the low-field spectral region. Between 4 and 18 °C there is no change in the number of resonances indicating that the structure is stable in this temperature range. Resonance line widths decrease, however, presumably due to decreasing correlation times at higher temperatures. Above 18 °C resonance intensity begins to decrease and the entire melting process is complete within 30 °C. Several distinct transitions are present in these data. For clarity we will, while considering these transitions, relate them immediately to those observed by optical studies as well as the NMR studies presented above.

Tertiary Structure. The first transition observed by optical studies (Table I) and NMR (Figures 3A and 4) has been attributed to the breaking of tertiary structure interactions between the D and TΨC loop regions. As seen in Table I, this transition has a slow relaxation rate and should be observed in low-field NMR spectra as a simple decrease in resonance intensity, without broadening, occurring at the previously observed T_m of 25 °C (Crothers et al., 1974). Figure 9a is a superposition of the 13 and 22 °C spectra from Figure 8. The blackened areas signal the first intensity decreases occurring at elevated temperatures. Two resonances are lost in region A, one in B, two in C, and one in E. When 10 mM cacodylate is used in place of 10 mM phosphate as the buffer, a clear resonance loss in region G at −11.6 ppm also occurs. In the present phosphate buffer, however, this appears only as a partial loss due to the shifting of a resonance just upfield of this peak. Romer and Varadi (1977), using solvent conditions also defined to resolve the tertiary structure melting, have observed these same intensity losses and assigned all losses to resonances from tertiary structure interactions. The regions where resonances from tertiary structure interactions are predicted (bottom, Figure 9b) agree with five of the seven resonances lost in this transition. Most noteworthy are the two resonances in region A assigned only by the new predictions to the two reversed Hoogstein tertiary structure interactions. The loss of the two resonances from peak C seems to be related to secondary structure changes rather than tertiary structure interactions and will be considered below.

In the region between −9 and −11 ppm four sharp resonances also begin to decrease in intensity very early, Figure 9a, and appear to be completely lost by 26 °C (see x in Figure 9b). They are also attributed to tertiary structure interactions and will be considered further in the Discussion.

The entire melting process observed in Figure 8 occurs over a temperature range of 25 °C and, unfortunately, it is not possible to avoid some overlap between the end of the first transition and the beginning of the second. Thus, in addition to the losses already noted in Figure 9a, a number of partial losses are distinctly visible before the end of the first transition at 26 °C. These are indicated by the arrows in Figure 9b. The intensity of these peaks indicates that approximately 30% of the melting in the second transition has occurred by 26 °C. As will be shown below in Figure 10, regions B, C, and E also contain resonances which melt out during the second transition. It is the partial melting of these resonances by 26 °C which accounts for the extra intensity lost in peaks B, C, and E of the difference spectrum, Figure 9b.

Accompanying the decrease in intensity in Figure 9b, two resonances report a structural change in the first transition, not by "melting" but by shifting their positions. As the intensity of the upfield side of peak B decreased, there is an increase of intensity on the low-field shoulder of this peak (see arrows in the 22 °C spectrum, Figure 8). Simultaneously, there is an increase in intensity in region G at ~−11.8 ppm which may correlate with some of the intensity lost in region C. These increases are the positive peaks (shaded area) in Figure 9b. As will be discussed later, these shifting resonances arise from secondary structure interactions which are reporting the breakdown of tertiary structure in transition 1.

Acceptor and Anticodon Helices. Transitions 2 and 3, observed optically (Table I) to occur at the same temperature, have been assigned to the opening of the acceptor and antico-

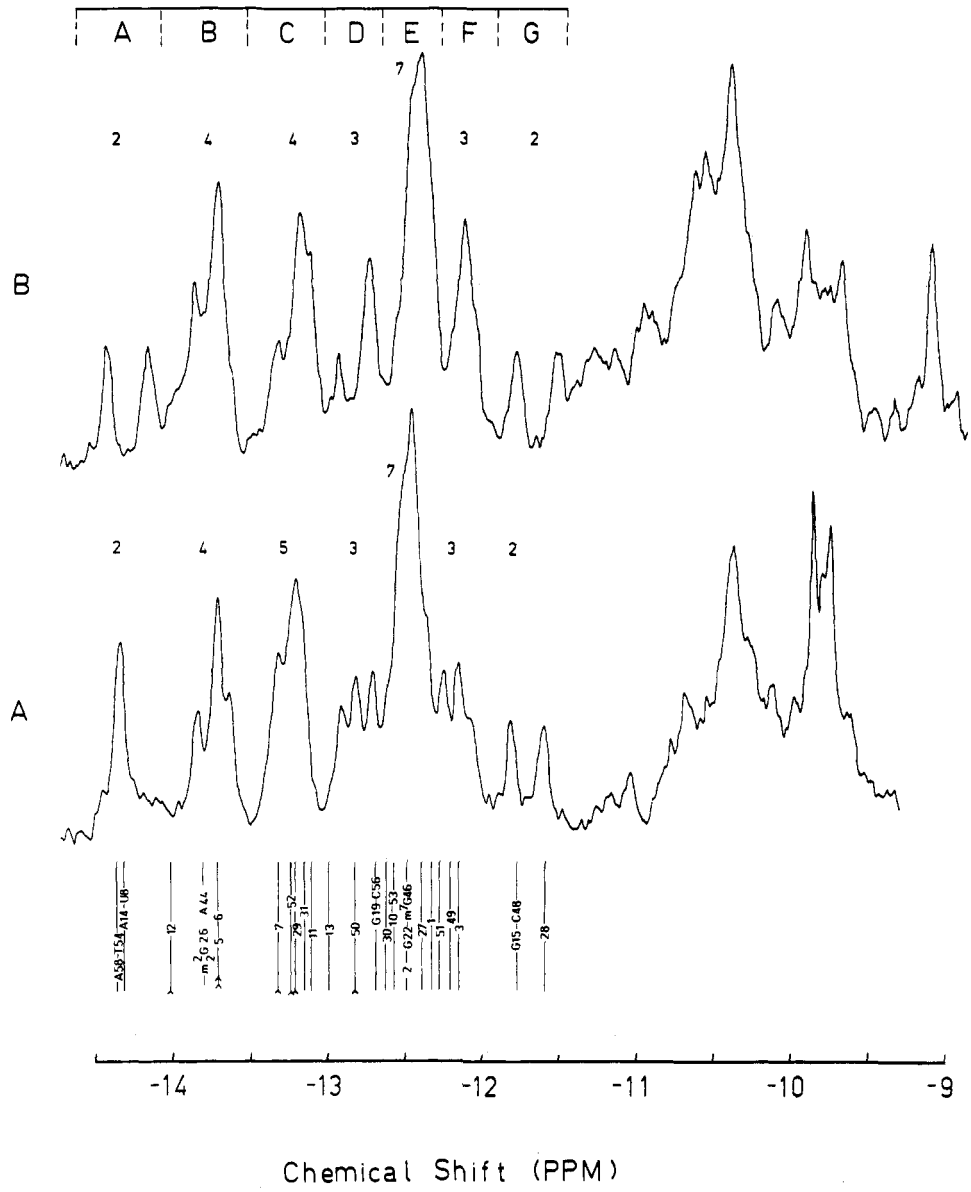

FIGURE 7: 360-MHz proton NMR spectra of the low-field spectral region of yeast $tRNA^{Phe}$ (5×10^{-4} M): (A) at 35 °C in 20 mM KH_2PO_4–5×10^{-4} M $MgCl_2$ (pH 6.8); (B) at 13 °C in 10 mM NaH_2PO_4–20 mM NaCl (pH 6.8), Mg^{2+} free. The numbers listed above the spectra represent the integrated intensities for the various regions in each spectrum. The resonance positions listed under spectrum A are the predictions arrived at by ring current calculations (Robillard et al., 1976b) based on atomic coordinates (Sussman & Kim, 1975).

don helices. Since the acceptor stem lacks methylated bases we observe this transition in Figure 3A, only for the anticodon helix. The relaxation times of these transitions are slow and, therefore, the transitions should be observed in the low-field spectra as losses in intensity without broadening at the T_m of 35 °C. Such a melting can be seen in Figures 8 and 10 where the results of subtracting the 26 °C from the 37 °C spectra are presented. At the bottom of Figure 10 we have marked the previously calculated positions of these two helices. It must be remembered that partial melting in this transition has already occurred by 26 °C; therefore, it is necessary to integrate within the 37–26 °C difference spectrum itself. On this basis we find a loss of two resonances in region B, one each in C and D, three in E, and one each in F and G. A total of 11 resonances are expected to melt in this transition while we observe a loss of 10. In regions C and D two resonances are lost where three were predicted to occur, while in the first transition, one more resonance melted from region C than was expected. The discrepancy lies, presumably, in the behavior of the A·Ψ resonance. Low-field spectra of the isolated anticodon fragment (Lightfoot et al., 1973) show the melting of one resonance in region C earlier than the rest and, because of its instability, it was assigned to the A·Ψ proton.

With this one justification the "melting" of the resonances in this transition fit well in number and reasonably well in predicted position with those resonances calculated for the acceptor and anticodon helices.

TΨC and D Helices. The last two transitions observed by the optical and NMR data (Table I and Figure 4) are the unwinding of the TΨC and D helices with the TΨC helix being somewhat less stable. Both transitions have fast relaxation rates and, following the treatment of Crothers et al. (1974) and Hilbers et al. (1976), should be observed as a simultaneous broadening and decrease in intensity of the hydrogen-bonded proton resonances. Broadening occurs when the helix lifetime is ~5 ms. On the high-temperature side of a transition the thermal relaxation time, τ, is dominated by the helix dissociation constant. At T_m, $2\tau = 1/K_d$. Extrapolating from the high-temperature relaxation times through 2τ at T_m to the 5-ms point gives the temperature at which the transition should

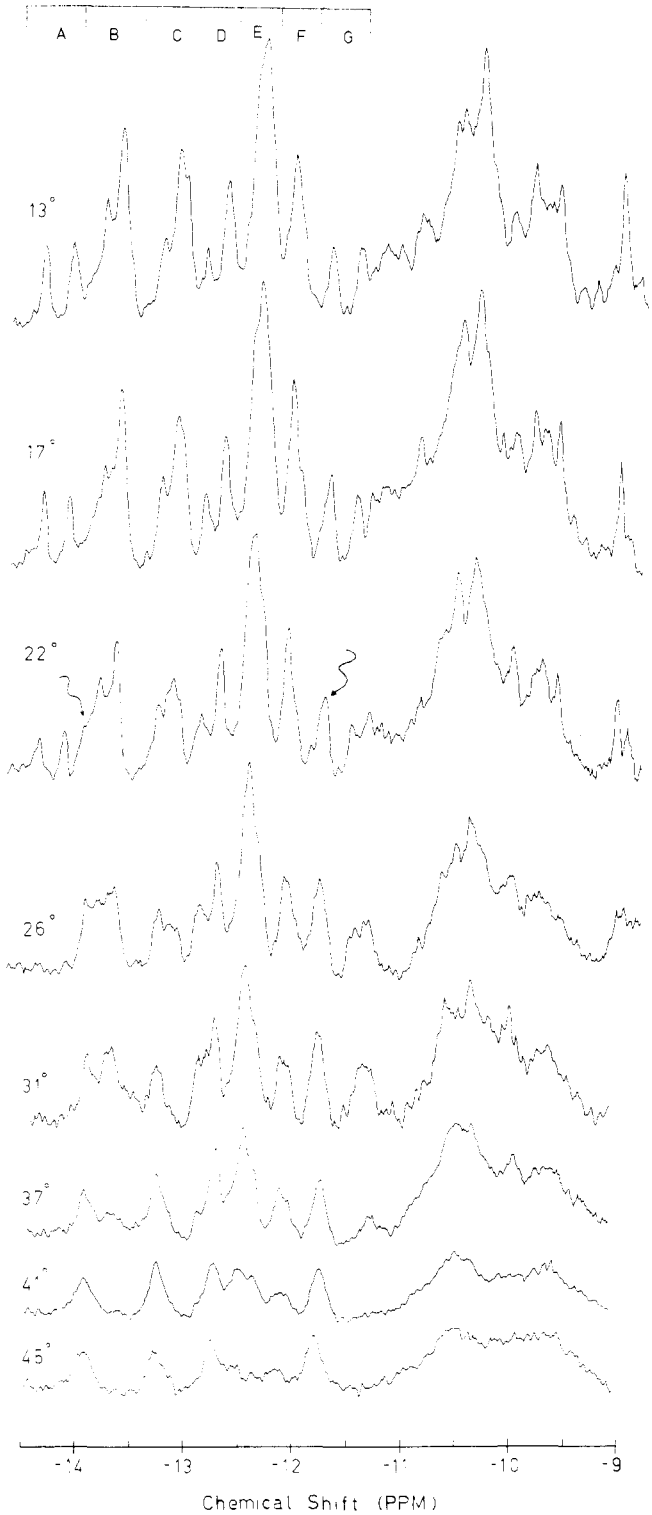

FIGURE 8: 360-MHz proton NMR spectra as a function of temperature for Mg^{2+} free yeast $tRNA^{Phe}$ in 10 mM NaH_2PO_4–20 mM NaCl (pH 6.8).

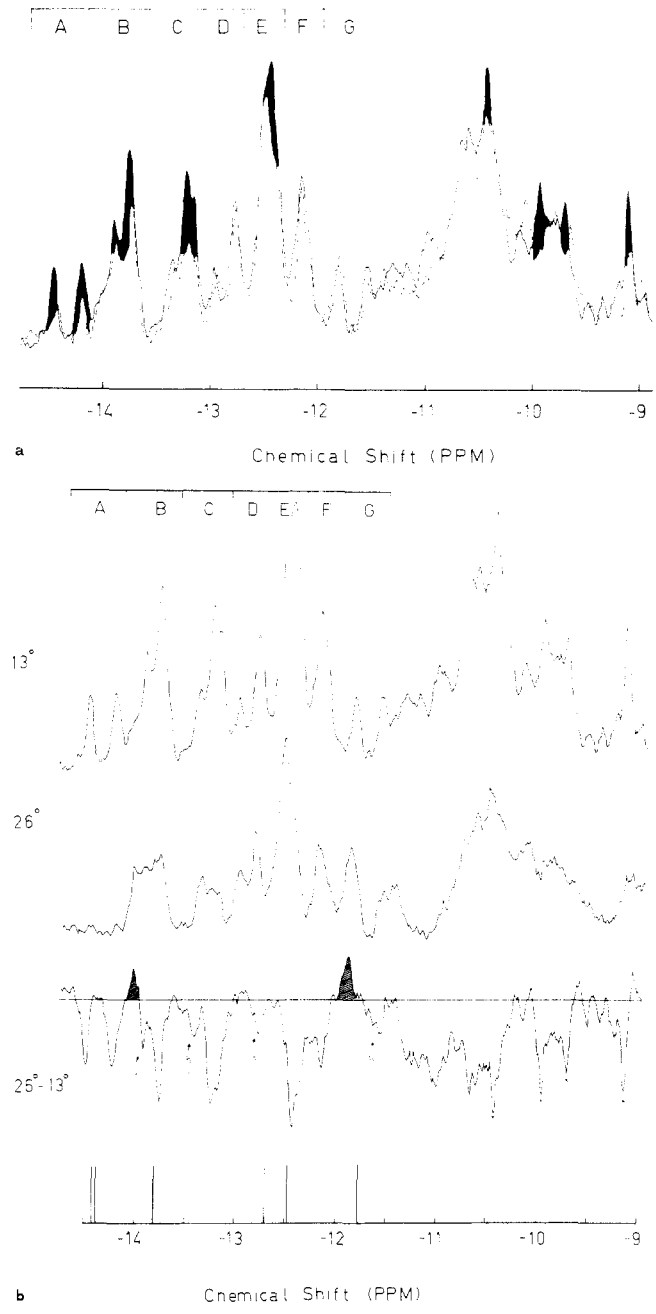

FIGURE 9: (a) Superposition of the 13 °C spectrum (solid line) and the 22 °C spectrum (dashed line) from Figure 8. The blackened area represents the major intensity losses between these two temperatures. (b) 13 and 26 °C spectra from Figure 8 plus a computer subtraction of the spectra. The negative peaks represent intensity lost by the transition from 13 to 26 °C. The lines at the bottom of the figure mark the positions attributed to tertiary structure resonances (see Figure 7).

be seen by NMR. Recalculating the published relaxation data for the CCA half-molecule in 0.11 M Na^+ (Romer et al., 1969) in this manner leads to the plot in Figure 11. The extrapolated temperature at which the TΨC helix lifetime is 5 ms is 40 °C. Therefore, broadening and subsequent melting of the TΨC helix resonances should be observed at or below 40 °C in the low-field spectral region. After the loss of the resonances from the acceptor and anticodon helices, eight or nine proton resonances remain (see Figure 8, 37 °C). Four or five of these resonances broaden and disappear between 37 and 45 °C as shown by the subraction in Figure 12. This transition occurs precisely in the manner expected from the relaxation studies on the CCA half-molecule and the extrapolation in Figure 11. The four clear resonance losses occur in regions D, E, and F in good agreement with the calculated positions for four of the TΨC resonances listed at the bottom of Figure 12. Whether or not the small negative peak in region B can be attributed to the A·U-52 base pair will be considered in the Discussion.

Unfortunately no thermal relaxation data for the pG half-molecule are available to construct a plot similar to Figure 11 for the D helix. The relaxation kinetics for this fragment, however, are essentially the same as for the CCA half-molecule

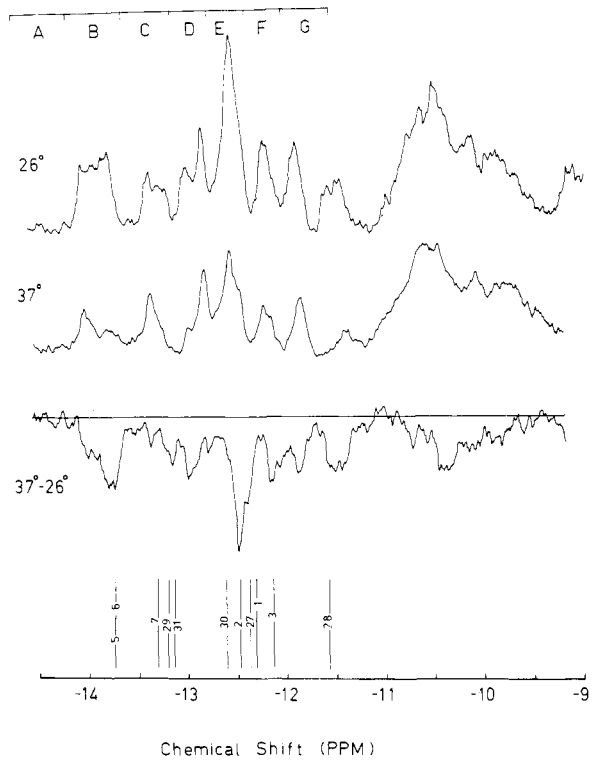

FIGURE 10: 26 and 37 °C spectra from Figure 8 plus a computer subtraction of the two spectra. The positions marked at the bottom of the figure are the calculated resonance positions of the Watson-Crick hydrogen-bonded protons of the acceptor stem and anticodon helix (see Figure 7).

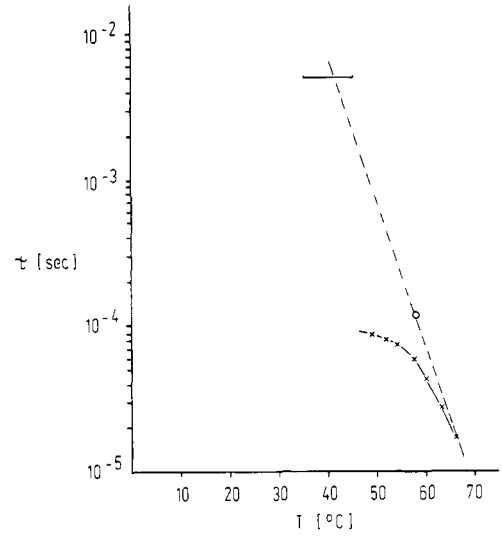

FIGURE 11: Plot of the change in relaxation time of the CCA half-molecule in 10 mM cacodylate-0.1 M NaCl (pH 6.8) as a function of temperature. The dashed line is drawn through the circle representing 2τ at $T = T_M$. The bar at 5 ms indicates the temperature region where broadening of the TΨC resonances is expected. The data for this figure are taken from Figure 3 of Romer et al. (1969).

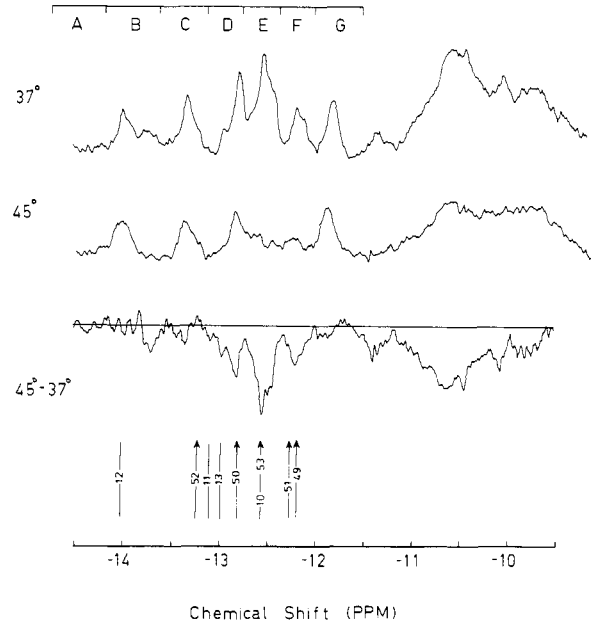

FIGURE 12: 37 and 45 °C spectra from Figure 8 plus a computer subtraction of these spectra. The positons marked at the bottom are those calculated for the Watson-Crick hydrogen-bonded protons of the TΨC and D helices (Figure 7). The TΨC resonance positions are marked by arrows.

(Romer et al., 1969) and, since it has a higher optical T_m, we can expect the same type of broadening and decreasing resonance intensities as observed for the TΨC resonances, but at a somewhat higher temperature. This is exactly what is observed. The 45 °C spectrum in Figure 12 contains only four resonances. It is the spectrum of the D helix. Proof of this can be found in published spectra of the 5′ half-molecule fragment which contains only the D helix (Lightfoot et al., 1973; Rordorf, 1975). The spectra of the 5′ half-molecule fragment are identical with the 45 °C spectrum presented above. The calculated positions in Figure 12 for A·U-12, G·C-11, and G·C-10 agree closely with observed positions. The resonance for G·C-13, however, is much further upfield than predicted. This discrepancy comes about because the predicted positions are based on atomic coordinates of the native tRNA where tertiary structure is intact, while, at 45 °C, all original tertiary structure is unfolded. We will treat this question in detail in the following paragraphs.

Discussion

Recently we proposed modified procedures for calculating hydrogen-bonded proton chemical shifts for tRNA NMR spectra (Robillard et al., 1976b, 1977). The purpose of the above presentation is to demonstrate that experimental evidence is available which supports these new calculations.

The application of proton NMR to the study of the physical chemical properties of nucleic acids has been advanced recently by the combination of NMR and temperature-jump relaxation data (Crothers et al., 1974; Hilbers et al., 1976). The range of relaxation rates for an individual transition monitored by temperature jump is related to the type of "melting" which should be observed in the low-field spectral region of tRNA NMR spectra. It is also possible to relate differential optical melting studies and NMR studies focusing on methyl resonances. The same events are reported by either technique. The unstacking of bases monitored by differential optical melting is reported as changes in hyperchromicity, while this same unstacking, monitored by NMR, is reported by changes in resonance positions for methyl group protons from the modified bases. Since there is less ambiguity in the assignment of methyl resonances than in the assignment of hydrogen-bonded proton resonances in tRNA NMR spectra, the most rational approach to assigning thermal transitions by NMR would be to first relate optical and NMR data from the methyl proton spectral region. Obviously this is only possible if there are a sufficient number of methylated bases evenly distributed throughout the molecule. Once these transitions have been defined the relax-

ation data from temp-jump measurements can be employed to predict how these transitions will manifest themselves in the temperature dependence of the hydrogen-bonded proton spectra. The NMR studies presented above have been performed under pH and ionic strength conditions identical with those employed throughout differential melting and temp-jump studies precisely to allow such a comparison.

Tertiary Structure. The principal alteration which we have made in the ring current prediction procedures is the change in the low-field starting positions for Watson–Crick and reversed Hoogstein A·U hydrogen-bonded proton resonances. By our procedure both proton resonances below −14 ppm are assigned to the two reversed Hoogstein tertiary interactions. All other prediction methods assign one or both of these resonances to secondary structure A·U hydrogen bonds from the acceptor stem. Therefore, one of the most direct tests of the validity of our procedure is to determine if these two resonances disappear at the time of the breakdown of tertiary structure. Before that, however, we must define when this transition occurs and it is for this reason that we focus on the high-field spectral region.

The transitions observed by optical and temp-jump techniques for yeast $tRNA^{Phe}$ in 30 mM Na (pH 6.8), no Mg^{2+}, are summarized in Table I. The most important of these transitions is the first. It is reported to be highly sensitive to Mg^{2+} and monovalent cations of varying ionic radii (Romer et al., 1970; Urbanke, et al., 1975). Stabilization of this transition stabilizes all subsequent transitions. A transition which has similar stabilizing effects has also been observed with the spin-labeled derivative, yeast $tRNA^{Phe}$ (-C-(s1)s^2C-A) (Sprinzl et al., 1974). Because of these properties, this transition has been assigned to the unfolding of tertiary structure. The breakdown of tertiary structure is clearly observable in Figure 3A by following the thymine resonance at 1 ppm. As the temperature is raised beyond 20 °C the resonance broadens and decreases in intensity. By 27 °C it is hardly visible, but it reappears, first broad, then sharper at 40 and 45 °C. This behavior is characteristic of a progression from slow exchange, through intermediate, to a fast exchange situation. The resonance assigned to the DHU in the 48 °C spectrum also undergoes a transition between 35 and 15 °C characteristic of a slow exchange conversion. As pointed out earlier both the T_m and the exchange characteristics indicate that this first transition observed by NMR is the same first transition observed optically, the breakdown of tertiary structure. These data indicate that the breaking of tertiary structure interactions will be manifested in the low-field spectral region as the first melting transition which will occur as a loss of resonance intensity without broadening at approximately 25 °C. This transition is clearly visible in Figures 8 and 9. The two reversed Hoogstein tertiaries were assigned to the −14.4-ppm resonances observed in spectra of yeast $tRNA^{Phe}$ in Mg^{2+} (see Figure 7) (Robillard et al., 1976b). In the absence of Mg^{2+} this resonance splits into two resonances. In support of our predictions, both resonances disappear during this transition. There is also a loss in regions B, E, and G where other tertiary interactions were predicted. In addition to the resonances between −11.5 and −15 ppm which are lost during transition 1, Figure 9 also shows the loss of at least four resonances in the region between −9 and −11 ppm. We have earlier associated resonances in the −11.5- to −10-ppm region with ring NH type interactions (Reid et al., 1975; Robillard et al., 1976a). Crystallographically observed tertiary structure interactions involving this type of bonding are G-15–C-48 and G-18–Ψ-55. The NH of Ψ-55 bonded to the oxygen of P-58 may also resonate in this spectral region. The second class of interactions which may contribute resonances in the region from −9 to −10.5 ppm is the exocyclic amino group protons directly bonded to a ring N such as A-9–A-23 and G-15–C-48. Recently, Steinmetz-Kayne et al. (1977) have observed pH-dependent intensity changes in the −9.9-ppm resonance and, from model studies, attributed this resonance to the A-9–A-23 tertiary interaction.

Resonance Assignments. The positions predicted for resonances from tertiary structure interactions (Figure 9b) were arrived at, in essence, by default. They were positions where no secondary structure resonances were calculated to occur (Robillard et al., 1976b). In view of this, the fact that there is such good agreement between predicted positions and observed intensity losses is itself a strong argument for the accuracy of the calculations. The low-field offsets of non-Watson–Crick type interactions are difficult to experimentally determine, however, making specific assignments problematical. With the exception of the two reversed Hoogstein and the G-19–C-56 interactions, the associations we have made of given tertiary interactions with specific resonances may well be altered by further detailed studies.

Secondary Structure. The arrows in the 22 °C spectrum of Figure 8 and the positive peaks in the difference spectrum of Figure 9b show that two resonances sense transition 1 not by disappearing but by changing position. These resonances most probably arise from protons in the D helix whose environment is altered upon the breakdown of tertiary structure. We know from crystallographic studies that bases in the TΨC and anticodon loops stack in a manner similar to the helical regions. In the D helix, however, as shown schematically in Figure 13A, the tertiary interaction with U-8 pulls the A-14 out from under the G·C-13 stack. Thus, with tertiary structure intact, A-14 contributes only 0.05-ppm upfield shift to the G·C-13 proton resonance resulting in a resonance at about −13.2 ppm as shown at the bottom of Figure 13A. When tertiary structure, including the U-8–A-14 interaction, unfolds at 25 °C (Figure 13B) A-14 should swing back stacking under G·C-13 contributing an additional upfield ring current shift to the G·C-13 resonance. In the resulting spectrum (bottom, Figure 13B) the resonance at −13.2 ppm disappears and a new one appears upfield. This accounts for the fact that the ring current calculation based on the crystal-structure coordinates predicts G·C-13 to occur in peak C or D while, in the fragment studies (Lightfoot et al., 1973; Rordorf, 1975) the G·C-13 resonance appears in region G where we also find it in the 45 °C spectrum of Figure 8.

The unfolding of tertiary structure is a slow relaxation process. Therefore, further spectral changes directly connected with this unfolding will have slow exchange characteristics if the chemical-shift difference between the initial and final states is greater than approximately 0.2 ppm. In agreement with these expectations the increase in intensity in region G of Figure 9b is accompanied by a simultaneous decrease in region C. A similar increase in resonance intensity on the low-field shoulder of peak B can be observed accompanying the decrease on the upfield side of this peak. This is the breakdown of tertiary structure being reflected in the A·U-12 resonance. A-23 participates in a tertiary structure interaction with A-9. The shifting of the A·U-12 resonance quite probably reflects a change in environment or charge distribution of A-23 when this tertiary interaction breaks. Such behavior of the A·U-12 resonance supports our interpretation of the G·C-13 shift.

Assignments via Melting and Fragment Studies. Shifting of the A·U-12 and G·C-13 resonances illustrates a serious problem in assigning hydrogen-bonded proton NMR spectra by melting studies. With covalently bonded protons, total

resonance intensity is conserved during the melting process, while with hydrogen-bonded protons, all resonance intensity is eventually lost. If it so happens that, due to some other structural change, a hydrogen-bonded proton resonance shifts from position 1 to position 2, while simultaneously some other resonance from another helix melts from position 2, the net change is −1 at position 1 and 0 at position 2. Therefore, one would assign the resonance at position 1 to the melting of the helix when in fact that resonance melted from position 2. In the cases we have pointed out above the shifts arose from the melting of tertiary structure. However, similar effects could also originate in the melting of specific elements of secondary structure. Assume, for example, that the solution structure of tRNA, after tertiary structure has melted, is represented by the four outstretched segments of the cloverleaf shown in Figure 13B. When the melting of the acceptor and antocodon stem occurs in the second transition A-66 will be freed to stack on base pair G·C-49 and m_2^2G-26 will be freed to stack on base pair G·C-10. Since the second transition is slow and the additional ring current effects are large, the resonances of G·C-10 and G·C-49 may change position in the slow exchange limit just as A·U-12 and G·C-13 have done. At first glance then it is surprising to see that the resonances for G·C-10 and G·C-49 seem to occur precisely where they are predicted using the ring current calculations based on the native tRNA structure (see Figure 12). In this case the agreement is fortuitous and arises because, in the native tRNA, the acceptor stem and TΨC helix form one continuous helix as do the D and anticodon helices. Therefore, in the native structure A-66 is fortuitously stacked on G·C-49 as is m_2^2G-26 on G·C-10 and the positions calculated from the intact structure will be the same as the resonance positions observed in the isolated helices in Figure 12. Such good fortune cannot be expected too often. Making assignments on the basis of fragment studies suffers these same difficulties as is clearly evident from the case of G·C-13 mentioned above. One cannot automatically work back from fragment spectra to making assignments of the intact molecule spectra with a higher degree of certainty than would be attainable by the reverse process.

Acceptor and Anticodon Helices. The observation that the acceptor and anticodon helices melt with the same T_m of 35 °C via processes with slow relaxation times agrees perfectly with the slow transition reported in Figure 3A for the anticodon methyl proton resonances. The hydrogen-bonded proton resonances lost at 35 °C (Figures 8 and 10) fit reasonably both in number and location to the calculated positions of resonances from protons in these two helices. Careful examination of the base stacking in the anticodon helix shows that the ring centers of G-43 and A-29 are both closer to the G·C-28 hydrogen-bonded proton than normally observed for an A-RNA helix. For this reason the shielding ring currents experienced by the G·C-28 proton from A-29 and G-43 are stronger than normal and the G·C-28 resonance is abnormally upfield shifted. It should be noted that calculations on partially refined coordinates of the MIT and MRC groups as well as the Duke group gave this same result (Robillard et al., 1977). It is, therefore, satisfying to note that a resonance is lost in this region during the transition assigned to the melting of the acceptor and anticodon helices.

TΨC and D Helices. Crothers et al. (1974) and Hilbers et al. (1976) have shown how it is possible to map an NMR "melting" onto a temp-jump relaxation experiment. Even without using NMR data from the methyl resonance region these mapping procedures would have predicted the melting behavior and T_ms observed in Figures 8 and 12. However, because they are directly comparable, the data from the methyl

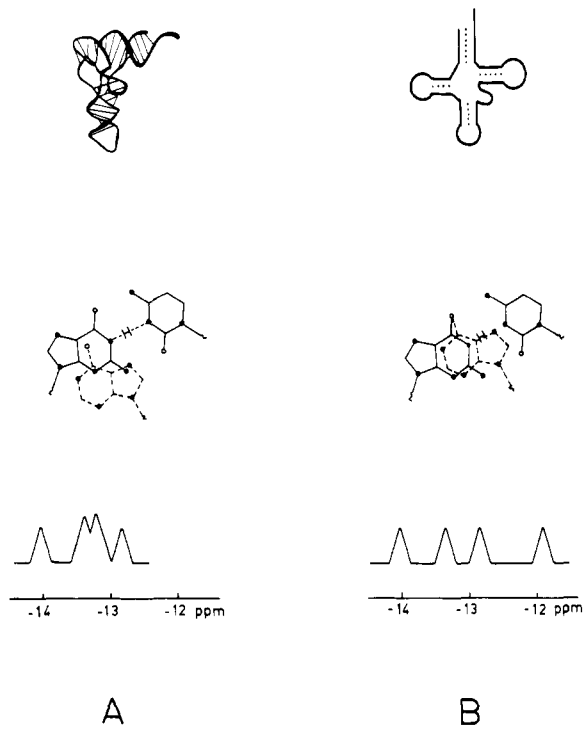

FIGURE 13: Schematic representation of the spectral shifts in the resonances from the D helix upon unfolding of tertiary structure: (A) with tertiary structure intact; the stacking arrangement for A-14 on G·C-13 is estimated from observations on the crystallographic structure; (B) with tertiary structure unfolded; the stacking arrangement estimated from plots of Arnott (1971) for an A'RNA helix.

resonance region confirm that the same processes monitored in the relaxation studies are also observed by NMR.

The temperature dependence of the DHU methylene resonance presented by Kan et al. (1974, 1977) is not in agreement with the data we present in Figure 4. They suggest that the m_2^2G-26 resonance stops shifting when it merges with the DHU resonance at about 60 °C and then the DHU resonance begins shifting. The double irradiation experiment in Figure 6 shows, however, that the m_2^2G-26 resonance shifts through the DHU peak and leaves the DHU resonance in the middle of the three peaks. This is also in agreement with the temperature-dependent shift of the other member of the DHU multiplet at −3.5 ppm. Both members of the multiplet should experience approximately the same shift and the same T_m in accord with what we present in Figure 4.

Agreement between Calculated and Observed Resonance Positions. The original spectral calculations (Robillard et al., 1976b) were carried out using coordinates with a crystallographic *R* factor of 39% (Sussman & Kim, 1975). It was recognized that inaccuracies either in the atomic coordinates or the ring currents and approximations used in the spectral calculations might lead to some errors in predicted resonance positions. Nevertheless, the expectation was that most resonances would occur at least in the same region where they were predicted. The present studies confirm that expectation. The predicted position of A·U-52 is an example of one of the few discrepancies which still exist. The A·U-52 resonance was predicted to occur in region C. However, no resonances from the TΨC helix seem to occur in this region. Some of the resonance shifts between regions may be due to the removal of Mg^{2+} which clearly causes a shift in region A. On the other hand, they could result from slow exchange changes which occur during the melting process itself as seen in the case of the A·U-12 and G·C-13 resonances. Considering the type of effects

TABLE II: Ring Current Calculated Methyl Resonance Positions.[a]

Base	Obsd position after RNase	+	Calcd shift	=	Calcd position	Obsd position intact tRNA
T-54	−1.87		0.831		−1.04	−1.02
m^5C-40	−1.95		0.363		−1.58	−1.54
m^5C-49	−1.95		0.261		−1.69	−1.63
$c^{11}Y$	−2.02		−0.014		−2.03	−2.09
m^2G-10	−2.90		0.101		−2.80	−2.80
Gm-34	−3.53		0.041		−3.49	−3.45
Cm-32	−3.58		0.003		−3.57	−3.65
m_2^2G-26	−3.10		0.528		−2.57	−2.48

[a] Calculated with optimized ring current values and procedures used previously (Robillard et al., 1976b, 1977).

which can complicate melting studies the agreement is good.

Local Structure Reflected in Resonances of Modified Bases. The assignments of the hydrogen-bond proton resonances given in Figure 8 were arrived at by ring current calculations of the NMR spectrum (Robillard et al., 1976b). It was recognized, however, that the base-paired hydrogen-bonded proton resonance positions were primarily sensitive to adjacent bases. Since few hydrogen bonds occur within the loop regions, the low-field spectral region provides very little information about the similarity between solution and crystallographic structure in loop regions. Using more recently refined coordinates (S. H. Kim, personal communication) ring current calculations were carried out to determine the shifts experienced by the methyl and methylene protons. The rotation of the methyl protons is accounted for by determining the shift experienced as they are rotated in 10° steps about the $X-CH_3$ bond. The final shift reported is simply the average of the shifts experienced at each step in rotation.

Table II compares the resonance positions of the methyl and methylene resonance between 0 and −3.5 ppm with those calculated from ring current shifts. There is excellent agreement between observed and calculated positions for all methyl groups monitored.

Resonance at 0 ppm. In Figures 3 and 4 a resonance occurs at 0 ppm for which we have, at present, no assignment. The resonance does not disappear after extensive dialysis and, furthermore, it has the same line width as the other resonances in the spectrum. The evidence that it is related to the tRNA is: (i) it disappears when the tRNA is treated with RNase (see Figure 5); (ii) it is present in commercial samples as well as those purified to homogeneity as described in this paper. Whether it arises from the tRNA or some persistent contaminant is still unclear.

Comparison with Other Studies. The assignment of the resonances below −14 ppm in the spectrum of yeast $tRNA^{Phe}$ has had a rather chaotic history. When the −14.4-ppm resonance was thought to be one proton it was assigned to A·U-6 (Lightfoot et al., 1973). In 1975 when the intensity jumped to 1.7 protons, a detailed ethidium bromide binding study was interpreted using A·U-6 and A·U-5 as the assignments (Jones & Kearns, 1975). Then came the solution of the x-ray crystal structure and the chemical modification studies to identify the resonances of the s^4U-8-A-14 tertiary. Alas, the assignment again changed to that for A·U-6 and U-8-A-14 hydrogen bonds (Wong & Kearns, 1974; Wong et al., 1975a,b). It should be evident that before NMR investigations into ligand binding sites, conformational changes, etc., are carried out, a consistent set of assignments is required. Such consistency has been lacking in the past. The original assignments based on fragment studies (Lightfoot et al., 1973) were not confirmed by subsequent melting studies (Hilbers et al., 1973). Furthermore, the interpretation of these melting studies did not agree with the transitions measured by optical and temp-jump techniques.

As a result of discrepancies uncovered while calculating ring current shifts using atomic coordinates for yeast $tRNA^{Phe}$ (Robillard et al., 1976b), we proposed a modified procedure for making assignment predictions. Without any changes in offsets or ring currents this procedure was successfully tested in calculating the NMR spectrum of *E. coli* $tRNA^{Val}_1$ (Robillard et al., 1977). The results presented in this paper represent another successful test of these procedures. After independently determining the order and characteristics of the low-field NMR melting transitions we found good agreement between the resonances influenced by individual transitions and their positions calculated by this modified procedure. The major difference between this procedure and the original one (Shulman et al., 1973) is that the low-field offset for Watson–Crick A·U resonances has been moved from −14.8 to −14.35 ppm. Under these conditions the A·U-6 resonance is calculated at −13.7 ppm and not −14.4 ppm. Furthermore, no secondary structure resonances are predicted at −14.4 ppm. This is in contrast to the assignments originating from earlier computational procedures. In agreement with our calculations both resonances below −14 ppm have melted by the time secondary structure begins to melt.

Geerdes and Hilbers (1977) have carried out ring current calculations also using atomic coordinates. In an attempt to experimentally determine the Watson–Crick and reversed Hoogstein A·U offsets they monitored the NH–N resonance positions of oligo(A)-oligo(U) duplexes and oligo(A)-$[oligo(U)]_2$ triplexes. In the duplex spectrum a single resonance was found whose position was −13.4 ppm. In the triplex spectrum two resonances were found at −13.47 and −13.25 ppm. The assumption was made that the resonances near −13.4 ppm in both spectra arose from one and the same Watson–Crick A·U interaction while the upfield resonance in the triplex spectrum arose from the reversed Hoogstein interaction. Unfortunately it is difficult to experimentally verify these assumptions. Nevertheless, using these assumptions Geerdes and Hilbers (1977) estimate a Watson–Crick A·U offset of −14.5 ppm and a reversed Hoogstein A·U offset of −14.5 ppm. A second equally plausible interpretation would have the Watson–Crick and reversed Hoogstein A·U offset of −14.3 ppm. A second equally plausible interpretation would have the Watson–Crick and reversed Hoogstein A·U offsets at −14.3 and −14.8 ppm, respectively, very close to the values we have found. Even with their preferred offsets, however, the calculated shifts do not correspond with observed resonance positions in the case of the U-8–A-14 and T-54–A-58 tertiaries and the A·U-6 secondary interactions.

Kan & Ts'o (1977) have also produced a set of ring current calculations using the Watson–Crick AU starting position of −14.7 selected by Kearns and Shulman (1974). They claim that, within a tolerance of 0.1 ppm, only four resonances out of 25 are incorrectly calculated. This claim, however, is based more on comparing calculated vs. observed resonance positions than on whether or not the correctly assigned resonance had been calculated to occur at the correct position. For instance, the two resonances below −14 ppm are, in Kan & Ts'o's calculations, assigned to secondary structure base pairs AU-6 and AU-12. These assignments are clearly incorrect. They are not secondary structure but, rather, tertiary structure resonances as shown by the results in this paper as well as those of Romer

& Varadi (1977) and Johnston & Redfield (1977) and the chemical modification studies of Reid et al. (1975) and Wong et al. (1975a). Since these two assignments, as well as the two AU tertiary structure resonances are misassigned by 0.5 ppm each, the errors in the calculations of Kan & Ts'o are substantially larger than they claim and it arises simply from the use of incorrect AU starting positions.

Romer and Varadi (1977) have recently carried out a study of the low-temperature melting behavior of yeast $tRNA^{Phe}$ in the absence of Mg^{2+} but at high sodium and cesium concentrations. Under these conditions the relaxation time of the tertiary structure transition is 1-2 ms and the resonances from tertiary structure interactions should broaden before melting. As temperature was raised they observed broadening and decreasing intensity of the same resonances which we observe to melt in Figure 9a. In our solvent the relaxation time is longer (10 ms) and the resonances should just decrease in intensity without broadening, precisely as we observed. Thus, there is complete agreement between the two sets of data relative to the positions, and exchange characteristics of the resonances involved in the tertiary structure transition.

Conclusions

The data presented above show that the positions predicted are consistent with experimental studies. In view of the success of these modified predictions both in these and earlier studies (Robillard et al., 1977) it appears that some assignments made in earlier studies may be incorrect and should be reexamined.

Acknowledgments

We wish to thank Professor G. Dirheimer for supplying some purified yeast $tRNA^{Phe}$. The cooperation of Dr. S. H. Kim in allowing us to examine, in detail, the fit of the electron density and atomic coordinates as well as supplying us with the latest refined atomic coordinates is gratefully acknowledged. We wish to express our appreciation to Dr. Kaptein and K. Dijkstra for technical assistance with the NMR spectrometer.

References

Arnott, S. (1971) *Prog. Biophys. Mol. Biol. 22,* 181-213.

Coutts, S. M., Riesner, D., Romer, R., Rabl, C. R., & Maass, G. (1975) *Biophys. Chem. 3,* 275-289.

Crothers, D. M., Cole, P. E., Hilbers, C. W., & Shulman, R. G. (1974) *J. Mol. Biol. 87,* 63-78.

Geerdes, H. A. M., & Hilbers, C. W. (1977) *Nucleic Acid Res. 4,* 207-221.

Giessner-Prettre, C., & Pullman, B. (1965) *C. R. Hebd. Seances Acad. Sci. 261,* 2521-2523.

Giessner-Prettre, C., & Pullman, B. (1970) *J. Theor. Biol. 27,* 87-95.

Gillam, T., Milleard, S., Blew, D., von Tigerstrom, M., Wimmer, E., & Tener, G. M. (1967) *Biochemistry 6,* 3043-3056.

Hilbers, C. W., Robillard, G. T., Shulman, R. G., Blake, D. R., Webb, P. K., & Riesner, D. (1976) *Biochemistry 15,* 1874-1882.

Hilbers, C. W., Shulman, R. G., & Kim, S. H. (1973) *Biochem. Biophys. Res. Commun. 55,* 953-960.

Holmes, W. M., Hurd, R. E., Reid, B. R., Rimerman, R. A., & Hatfield, W. (1975) *Proc. Natl. Acad. Sci. U.S.A. 72,* 1068-1071.

Johnston, P. D., & Redfield, A. G. (1977) *Nucleic Acids Res.* (in press).

Jones, C. R., & Kearns, D. R. (1975) *Biochemistry 14,* 2660-2665.

Kan, L. S., & Ts'o, P. O. P. (1977) *Nucleic Acids Res. 4,* 1633-1647.

Kan, L. S., Ts'o, P. O. P., Sprinzl, M., Van der Haar, F., & Cramer, F. (1977) *Biochemistry 16,* 3143-3153.

Kan, L. S., Ts'o, P. O. P., Van der Haar, F., Sprinzl, M., & Cramer, F. (1974) *Biochem. Biophys. Res. Commun. 59,* 22-29.

Kearns, D. R., & Shulman, R. G. (1974) *Acc. Chem. Res. 7,* 33-39.

Kim, S. H., Suddath, F. L., Quigley, G. J., McPherson, A., Sussman, J. S., Wang, A. H. J., Seeman, N. C., & Rich, A. (1974) *Science 185,* 435-440.

Koehler, K. M., & Schmidt, P. G. (1973), *Biochem. Biophys. Res. Commun. 50,* 370-376.

Lightfoot, D. R., Wong, K. L., Kearns, D. R., Reid, B. R., & Shulman, R. G. (1973) *J. Mol. Biol. 78,* 71-89.

Nishimura, S. (1971) *Proced. Nucleic Acid Res. 2,* 542-564.

Reid, B. R., Ribeiro, N. S., Gould, G., Robillard, G. T., Hilbers, C. W., & Shulman, R. G. (1975) *Proc. Natl. Acad. Sci. U.S.A. 72,* 2049-2053.

Reid, B. R., Ribeiro, N. S., McCollum, L., Abbate, J., & Hurd, R. E. (1977) *Biochemistry 16,* 2086-2094.

Reid, B. R., & Robillard, G. T. (1975) *Nature (London) 257,* 287-291.

Riesner, D., Maass, G., Thiebe, R., Philippsen, P., & Zachau, H. (1973) *Eur. J. Biochem. 36,* 76-88.

Robertus, J. D., Ladner, J. E., Finch, J. T., Rhodes, D., Brown, R. S., Clark, B. F. C., & Klug, A. (1974) *Nature (London) 250,* 546-551.

Robillard, G. T., Hilbers, C. W., Reid, B. R., Gangloff, J., Dirheimer, G., & Shulman, R. G. (1976a) *Biochemistry 15,* 1883-1888.

Robillard, G. T., Tarr, C. E., Vosman, F., & Berendsen, H. J. C. (1976b) *Nature (London) 262,* 363-369.

Robillard, G. T., Tarr, C. E., Vosman, F., & Sussman, J. L. (1977) *Biophys. Chem. 6,* 291-298.

Romer, R., Riesner, D., & Maass, G. (1970) *FEBS Lett. 10,* 352-357.

Romer, R., Riesner, D., Maass, G., Wintermeyer, W., Thiebe, R., & Zachau, H. G. (1969) *FEBS Lett. 5,* 15-19.

Romer, R., & Varadi, V. (1977) *Proc. Natl. Acad. Sci. U.S.A. 74,* 1561-1564.

Rodorf, B. F. (1975) Ph.D. Thesis, Department of Chemistry, University of California, Riverside, Calif.

Schmidt, J., Wang, R., Stanfield S., & Reid, B. R. (1971) *Biochemistry 10,* 3264-3268.

Shulman, R. G., Hilbers, C. W., Kearns, D. R., Reid, B. R., & Wong, Y. P. (1973) *J. Mol. Biol. 78,* 57-68.

Smith, I. C., Yamane, T., & Shulman, R. G. (1969) *Can J. Biochem. 47,* 480-484.

Sprinzl, M., Kramer, E., & Stehlik, D. (1974) *Eur. J. Biochem. 49,* 595-604.

Steinmetz-Kayne, M., Benigno, R., & Kallenbach, N. R. (1977), *Biochemistry 16,* 2064-2073.

Sussman, J. L., & Kim, S. H. (1975) *Biochem. Biophys. Res. Commun. 68,* 89-95.

Urbanke, C., Romer, R., & Maass, G. (1975) *Eur. J. Biochem. 55,* 439-444.

Wong, K. L., Bolton, P. H., & Kearns, D. R. (1975a) *Biochim. Biophys. Acta 383,* 464-451.

Wong, K. L., & Kearns, D. (1974) *Nature (London) 252,* 738-739.

Wong, K. L., Kearns, D. R., Wintermeyer, W., & Zachau, H. G. (1975b) *Biochim. Biophys. Acta 395,* 1-4.